

Journal of Biomedical Optics

SPIEDigitalLibrary.org/jbo

Enhanced fluorescence diffuse optical tomography with indocyanine green-encapsulating liposomes targeted to receptors for vascular endothelial growth factor in tumor vasculature

Saeid Zanganeh
Yan Xu
Carl V. Hamby
Marina V. Backer
Joseph M. Backer
Quing Zhu

Enhanced fluorescence diffuse optical tomography with indocyanine green-encapsulating liposomes targeted to receptors for vascular endothelial growth factor in tumor vasculature

Saeid Zanganeh,^a Yan Xu,^a Carl V. Hamby,^b Marina V. Backer,^c Joseph M. Backer,^{c,*} and Quing Zhu^{a,*}

^aUniversity of Connecticut, Departments of Bioengineering and Electrical and Computer Engineering, Storrs, Connecticut 06269

^bNew York Medical College, Department of Microbiology and Immunology, Valhalla, New York 10595

^cSibTech, Inc., 115A Commerce Drive, Brookfield, Connecticut 06804

Abstract. To develop an indocyanine green (ICG) tracer with slower clearance kinetics, we explored ICG-encapsulating liposomes (Lip) in three different formulations: untargeted (Lip/ICG), targeted to vascular endothelial growth factor (VEGF) receptors (scVEGF-Lip/ICG) by the receptor-binding moiety single-chain VEGF (scVEGF), or decorated with inactivated scVEGF (inactive-Lip/ICG) that does not bind to VEGF receptors. Experiments were conducted with tumor-bearing mice that were placed in a scattering medium with tumors located at imaging depths of either 1.5 or 2.0 cm. Near-infrared fluorescence diffuse optical tomography that provides depth-resolved spatial distributions of fluorescence in tumor was used for the detection of postinjection fluorescent signals. All liposome-based tracers, as well as free ICG, were injected intravenously into mice in the amounts corresponding to 5 nmol of ICG/mouse, and the kinetics of increase and decrease of fluorescent signals in tumors were monitored. A signal from free ICG reached maximum at 15-min postinjection and then rapidly declined with $t_{1/2}$ of ~ 20 min. The signals from untargeted Lip/ICG and inactive-Lip/ICG also reached maximum at 15-min postinjection, however, declined somewhat slower than free ICG with $t_{1/2}$ of ~ 30 min. By contrast, a signal from targeted scVEGF-Lip/ICG grew slower than that of all other tracers, reaching maximum at 30-min postinjection and declined much slower than that of other tracers with $t_{1/2}$ of ~ 90 min, providing a more extended observation window. Higher scVEGF-Lip/ICG tumor accumulation was further confirmed by the analysis of fluorescence on cryosections of tumors that were harvested from animals at 400 min after injection with different tracers. © 2013 Society of Photo-Optical Instrumentation Engineers (SPIE) [DOI: 10.1117/1.JBO.18.12.126014]

Keywords: fluorescence diffuse optical tomography; contrast agent; indocyanine green-encapsulating liposomes; vascular endothelial growth factor receptors-targeting liposome; single-chain version of vascular endothelial growth factor.

Paper 130431R received Jun. 22, 2013; revised manuscript received Oct. 25, 2013; accepted for publication Nov. 18, 2013; published online Dec. 17, 2013.

1 Introduction

Near-infrared fluorescence diffuse optical tomography (FDOT) is an emerging imaging technique that provides depth-resolved spatial distributions of fluorescence in tumor.^{1–12} The FDOT has been explored for imaging endogenous fluorescence, as well as molecular probe fluorescence in small animals,^{1–7} and in human brain and breast tumors.^{8–10} The biggest challenge for clinical applications is to develop imaging techniques and fluorescent tracers that allow for imaging of deeply seated tumors with high sensitivity and within convenient postinjection time window.^{11–13}

Indocyanine green (ICG) is a fluorescence dye with desired absorption and emission spectra in the near-infrared optical window (600 to 900 nm), and it is approved for clinical use since 1959.^{14,15} Intravenously injected ICG rapidly binds to serum proteins, mostly to albumin, and the complexes transiently accumulate in tumors via nonspecific enhanced permeability and retention (EPR) effect due to the leaky tumor vasculature¹⁶ and then rapidly cleared from tumor area with blood half-life

in humans of ~ 25 min only.¹⁷ This rapid clearance stimulated development of various novel ICG formulations, and significant sensitivity advantages and prolonged labeling of tumors have been reported recently for ICG-encapsulating lipid nanoparticles¹⁸ and liposomes.¹⁹ The observed effects are most likely due to a more significant EPR-based accumulation of these constructs relative to ICG/protein complexes. Interestingly, detailed spectroscopic studies of liposome-encapsulated ICG revealed a small but significant red shift in absorption and emission peaks for encapsulated versus free ICG.¹⁹

A recent report on the enhanced binding of cetuximab-targeted ICG-encapsulating liposomes to cancer cells overexpressing receptors for epidermal growth factor²⁰ suggests that molecular targeting of liposome-encapsulated ICG (Lip/ICG) to tumor-related receptors could further enhance tracer accumulation or retention in tumor beyond EPR-related levels. However, liposomes targeted to tumor-specific receptors still have to extravasate through tumor blood vessels and to diffuse through tumor interstitial space, the processes that do not allow for a dramatic increase in their tumor accumulation relative to

*Address all correspondence to: Joseph M. Backer, E-mail: jbacker@sibtech.com; Quing Zhu, E-mail: zhu@engr.uconn.edu

that based on EPR. Indeed, liposomes typically do not diffuse into tumor interstitial space beyond one or two layers of sub-endothelial cells, and even in this compartment, they are rapidly cleared by tumor resident macrophages.²¹

We hypothesized that targeting Lip/ICG to vascular endothelial growth factor receptors (VEGFRs) expressed on tumor endothelial cells might significantly enhance and/or prolong tracer accumulation in the tumor relative to that based on EPR effect or targeting tumor cells. Indeed, although tumor endothelial cells constitute only a small fraction (1% to 5%) of all cells in tumors, their receptors are accessible directly from blood flow and therefore targeting of Lip/ICG to VEGFRs would not depend on tumor vessel extravasation, diffusion through tumor interstitium, and clearance by tumor resident macrophages.

To test this hypothesis, we have developed a novel targeted fluorescent tracer for FDOT, scVEGF-Lip/ICG, targeted to VEGFRs in tumor vasculature. For targeting, Lip/ICG were decorated with previously described scVEGF-PEG-DSPE, an engineered single-chain version of vascular endothelial growth factor (scVEGF), site-specifically derivatized with PEGylated lipid for coupling to liposomes.^{22,23} We have previously described scVEGF-based nuclear and fluorescent tracers, as well as lipid microbubbles-based ultrasound (US) tracers, for VEGFR imaging in angiogenic vasculature in various pathologies.^{22–27} High-affinity binding of these tracers to VEGFRs has been validated by positron emission tomography, single-photon emission computed tomography, US, and near-infrared fluorescence imaging of VEGFR in various cancer, cardiovascular, and inflammation models.^{25,27–30}

Here, we used scVEGF-Lip/ICG for FDOT imaging of VEGFRs in tumor-bearing mice with orthotopic mammary carcinoma. To evaluate nonspecific tracer accumulation via EPR, we used free ICG and untargeted Lip/ICG. An additional control, inactive-Lip/ICG, decorated with inactivated scVEGF, was used to assess how the decoration of Lip/ICG with a functionally inactive protein can affect EPR-based tracer accumulation.

Using FDOT imaging of tumor-bearing mice with orthotopic mammary carcinoma, we found that all tracers transiently accumulate in the tumor area. In agreement with our hypothesis, scVEGF-Lip/ICG displayed the superior characteristics with respect to the accumulation rate and retention in tumor area by FDOT imaging, which were confirmed by the analysis of fluorescence in tumor cryosections.

2 Materials and Methods

2.1 Reagents

Laser-grade ICG (IR-125) was from Acros Organics (Pittsburgh, Pennsylvania). Chloroform solutions of lipids DOPC (1,2-dioleoyl-*sn*-glycero-3-phosphocholine), DOPE (1,2-dioleoyl-*sn*-glycero-3-phosphatidylethanolamine), and DOPE-PEG-2000 (1,2-dioleoyl-*sn*-glycero-3-phosphatidylethanolamine-*N*-[poly(ethylene-glycol) 2000]) were from Avanti Polar Lipids (Alabaster, Alabama), chloroform solution of cholesterol was from Supelco (Bellefonte, Pennsylvania), and cyclohexane was from Acros. DSPE-PEG(3.4 kDa)-maleimide (1,2-distearoyl-*sn*-glycero-3-phosphoethanolamine-*N*-[amino(polyethylene glycol)-3,400]-maleimide) was from Nektar (Huntsville, Alabama). DMSO (dimethyl sulfoxide) was from Pierce (Rockford, Illinois). [C4]monothiol scVEGF (single-chain human vascular endothelial

growth factor) and VEGF-SLT fusion toxin were available from SibTech, Inc. (Brookfield, Connecticut).

2.2 Preparation of Tracers

Phospholipids and cholesterol in chloroform were mixed at the following molar percent ratio: DOPE (31):Cholesterol (33.5):DOPC (31):DOPE-PEG-2000 (2.5) and evaporated under vacuum for 1 h. To remove residual chloroform, cyclohexane was added to dry lipid/cholesterol film, vortexed for 1 min, and evaporated under vacuum for 1 h. The ICG was added to dry lipid as a stock solution in methanol (5 to 7 mg/ml) and vortexed for 1 min to ensure efficient mixing of lipids/cholesterol film with the dye. Methanol was then evaporated under vacuum for 16 h in the dark. Dry lipid/cholesterol/ICG film was hydrated in a buffer containing 10-mM HEPES (pH 7.2), 150-mM NaCl, 0.2-mM EDTA, passed through three cycles of freezing at liquid nitrogen and thawing at 58°C, and 25-cycles of extrusion through 80-nm pore diameter membranes at 58°C. The resulting unilamellar liposomes were purified by size-exclusion chromatography on Sepharose 4B (Sigma, St Louis, Missouri). The concentration of liposome-entrapped ICG was determined in methanol lysates by the absorbance at 784 nm with stock ICG solution in methanol serving as a standard. This procedure led to 75% to 90% encapsulating of ICG, yielding a concentration within 2 to 3 mM. For surface decoration of liposomes with functionally active scVEGF, [C4]-monothiol-scVEGF was site-specifically lipidated with 2 to 4 molar excess DSPE-PEG(3.4 kDa)-maleimide dissolved in DMSO for 10 min at room temperature (RT). The entire lipidation reaction was mixed with purified liposomes at an average scVEGF-to-phospholipid molar ratio of 1:150 and incubated for 12 to 14 h at 37°C. scVEGF-decorated liposomes were purified from free protein by size-exclusion chromatography on Sepharose 4B. The concentration of scVEGF was determined by SDS-PAGE with free scVEGF serving as a standard. An average concentration of liposome-associated scVEGF was 2 to 4 μ M.

To prepare inactive-Lip/ICG, scVEGF moiety in lipidated scVEGF was inactivated, as was described previously for other scVEGF-based tracers¹⁹ by biotinylation of lysine residues. Briefly, scVEGF site-specifically derivatized with DSPE-PEG (3.4 kDa) as described above and was incubated with a 100-fold molar excess of biotin-NHS ester (Invitrogen, Grand Island, New York) for 30 min at RT. Unreacted NHS was quenched by incubation with a 12-fold molar excess (relative to biotin-NHS) of Tris-HCl at pH 8.0. The resulting biotinylated scVEGF-lipid conjugate was used for decorating Lip/ICG, as described above, yielding inactive-Lip/ICG tracer.

2.3 Tissue Culture

All cell lines were from SibTech, Inc. 4T1luc cells, a luciferase-expressing derivative of 4T1 mouse mammary carcinoma cells, were used to establish orthotopic tumors in Balb/c mice. PAE/KDR cells, porcine aortic endothelial cells expressing $\sim 10^5$ VEGFR-2 per cell, were used for flow-cytometry analysis of Lip/ICG and scVEGF-Lip/ICG bindings. 293/KDR cells, human embryonic kidney cells expressing $\sim 2.5 \times 10^5$ VEGFR-2 per cell, were used for the evaluation of VEGFR-2-binding and activation activities of scVEGF-Lip/ICG. 4T1luc cells were maintained in RPMI 1640 medium (Gibco, Grand Island, New York). VEGFR-2 expressing cells were maintained in high-glucose DMEM (Gibco). All media were supplemented

with 10% FBS, 50-U/ml penicillin/streptomycin, 2-mM L-glutamine, and 1-mM pyruvate. Cells were routinely cultured at 37°C and 5% CO₂.

2.4 Induction of VEGFR-2 Tyrosine Phosphorylation

Previously described protocol²² was used with minor modifications. Briefly, 293/KDR cells were seeded on 24-well plates at 60,000 cells/well, 18 to 20 h before the assay. Varying amounts of scVEGF-Lip/ICG or free scVEGF diluted in complete culture medium were added to cells and incubated for 10 min at 37°C; then, the media were aspirated, and cells were lysed and analyzed by Western blotting with phosphotyrosine antibody specific to Y1175 of VEGFR-2 (Cell Signaling, Danvers, Massachusetts) with chemiluminescent development using ECL Plus kit (GE Healthcare, Piscataway, New Jersey). After development, the blot was stripped and reprobed with antibody specific to total VEGFR-2 (Santa Cruz Biotechnology, Dallas, Texas). To ensure equal protein loading, same lysates were analyzed by Western blotting with β -actin-specific antibody (Sigma).

2.5 Competition with VEGF-Toxin (SLT-VEGF)

Previously described protocol²² was used with minor modifications. Briefly, 293/KDR cells were plated on 96-well plates at 2,000 cells/well, 18 to 20 h before the exposure. scVEGF-Lip/ICG or free scVEGF was serially diluted with complete culture medium containing SLT-VEGF and added to cells in triplicate wells to a final concentration of 1 nM for SLT-VEGF and final concentration of scVEGF ranging from 0 to 25 nM. After 96 h of incubation under normal culture conditions, viable cells are determined by CellTiter 96(R) Aqueous Non-Radioactive Proliferation Assay (Promega, Madison, Wisconsin). The number of viable cells indicates the ability of scVEGF to compete with SLT-VEGF for binding to VEGFR-2 and thus determines its functional activity.

2.6 Flow Cytometry

PAE/KDR cells were plated in T25 flasks, 1 ml/flask, 20 h before the assay. Targeted scVEGF-Lip/ICG was added to one flask to a final concentration of 2.5-nM scVEGF and 2- μ M ICG. Nontargeted liposomes Lip/ICG were added to another flask to a final ICG concentration of 2 μ M. Cells were incubated for 1 h under normal culture conditions; then, the media were aspirated, and the cell was extensively washed, detached from plastic with PBS/EDTA (Gibco), and fixed with 4% formaldehyde for 5 min at room temperature. Flow cytometry was performed with a MACSQuant cytometer (Miltenyi Biotech, Auburn, California) equipped with violet (405 nm), blue (488 nm), and red (635 nm) lasers. Fluorescent events were acquired, and data files were analyzed with MACSQuantify™ software (Miltenyi Biotech, Auburn, California). Cell events visualized by forward and side scatter plots were gated to exclude cell debris and clumped cells were then analyzed for fluorescent intensity. Histogram plots of cells without liposomes, untargeted Lip/ICG, and scVEGF-Lip/ICG were overlaid to show the distribution of fluorescence intensity for each cell population.

2.7 Animal Protocol

In vivo experiments were performed using an orthotopic murine breast tumor model. The animal protocol was approved by the Institutional Animal Care and Use Committee of University of

Connecticut. 4T1luc cells grown in T75 flasks (BD Biosciences, Bedford, Massachusetts) to the 75% to 80% confluence were used for injection into animals. To obtain orthotopic tumors, 4T1luc cells were injected into the lower right mammary fatpad of 7-week-old Balb/c female mice, 10⁵ cells per mouse. The imaging experiments were performed when the tumor sizes reached approximately 6 to 7 mm in diameter, 2 to 3 weeks post-inoculation. All experiments were performed with mice under anesthesia induced by inhaling 1.5% isoflurane.

For histology, harvested tumors, after overnight fixation in 4% paraformaldehyde (PFA), were dehydrated progressively through 30%, 50%, 70%, 90%, and 100% ethanol and then placed in OCT embedding medium (Tissue-Tek, Torrance, California). Tumor samples, sectioned at 10 μ m on a cryostat (Leica CM3050S, Leica Microsystems, Nussloch, Germany), were stored at -20°C.

2.8 FDOT System and Animal Experiments

The *in vivo* experiments were performed using a frequency domain fluorescence imaging system, which consisted of 14 parallel detectors and 4 laser diodes of 690, 780, 808, and 830 nm.³¹ Each laser diode was sequentially switched to nine positions on a hand-held probe (see Fig. 1). In this study, 690 nm was used as the excitation wavelength. The emission bandpass filter has the center wavelength of 800 nm and the band width of 60 nm. Thus, the 690 nm is the most proper choice for the excitation. The 14-channel parallel detection system has two modes: fluorescence and absorption modes. The two modes can be easily switched by moving a mechanical handle. A stopper was designed in the system to ensure a precise optical collimation when switching between these two modes. Note that in the fluorescence mode, a bandpass filter was placed in the light path to remove the excitation and stray light. In the absorption mode, the bandpass filter was moved out of the light path. Fourteen photomultiplier tubes were used as detectors, and the received signals were amplified by preamplifiers, mixed by mixers, low-pass filtered, and further amplified before analog to digital converters. Two National Instrument data acquisition cards of 8-channels each were used to acquire FDOT data.

For imaging experiments, an anesthetized mouse was mounted on a thin glass plate facing the probe with the lower mammary pads submerged in the Intralipid solution of typical soft tissue absorption coefficient $\mu_a = 0.02$ to 0.03 cm⁻¹ and reduced scattering coefficient $\mu'_s = 6$ to 7 cm⁻¹. In the experiment, the center of the probe was aligned to the center of the tumor, and the separation between the tumor center and the probe surface was defined as the imaging depth for

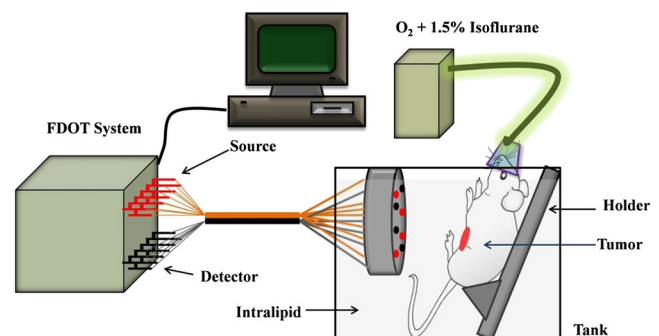


Fig. 1 *In vivo* fluorescence imaging setup.

fluorescence images. Anesthetized mice were intravenously injected with 100- μ l solution containing 5 nmol of ICG in targeted and untargeted formulations. During experiments, the tumor was imaged in each anesthetized mouse at 1, 15, 30, 60, and 90 min. Beyond 90 min, the animals were given an anesthesia break and imaged again at 2.5, 3.5, 4.5, 5.5, and 6.7 h with anesthesia breaks in between.

2.9 Fluorescent Images of Tumor Samples

Tumors were harvested at 400 min after tracer injection, and 10- μ m tumor cryosections were cut to represent all parts of each tumor. Frozen tumor cryosections were dried and imaged by an Odyssey Infrared Imaging System (Li-COR Biosciences, Lincoln, Nebraska). This instrument provides scan resolution ranging from 21 to 339 μ m. The fluorescence images obtained for this work were acquired at the highest resolution of 21 μ m. The selected excitation channel was 785 nm and emission channel was 820 nm with a bandwidth of 40 to 50 nm. All samples in this study were imaged using the same setup parameters for the Odyssey Infrared Imaging System in terms of resolution, brightness, and contrast. Cryosection images were converted in Adobe Photoshop to grayscale and binarized to black (background) and white (ICG stained) pixels at the same threshold level for all images, and a percentage of white pixels on each image was determined by histogram analysis.

2.10 Statistical Analysis

A two-sample two-sided *t*-test was used to calculate the statistical significance for comparisons between the three control groups and the targeted group injected with scVEGF-Lip/ICG, and a difference with a *P*-value of less than 0.05 was considered to be significant.

2.11 Image Reconstruction

To reconstruct fluorescence images, a normalized Born approximation has been widely used.^{32,33} This normalization eliminates unknown system parameters such as source strengths, gains of different detectors, background optical properties of the tissue, coupling efficiency to the tissue, etc. This normalized Born ratio was adopted in our earlier studies²⁴ and is given as

$$\phi^{\text{NB}}(r_s, r_d) = \frac{\phi_{\text{fl}}(r_s, r_d)}{\phi_{\text{exc}}(r_s, r_d)}, \quad (1)$$

where ϕ^{NB} is the normalized Born ratio, ϕ_{fl} is the fluorescence measurement after subtraction of the system noise measurement without any fluorophores or targets in the background medium, and ϕ_{exc} is the excitation measurement at 690 nm. For inversion, a dual-zone mesh method was used to reconstruct the fluorophore concentrations at the target depth, and the background regions and the details were given in our early publications.^{24,34} Briefly, we divide the imaging region into two parts: the background (B) and target (T) regions. Therefore, Eq. (1) can be further expressed as a matrix equation when multiple measurements are available

$$[M]_{V \times 1} = [W_T, W_B]_{V \times N} [X_T, X_B]_{N \times 1}, \quad (2)$$

where M is the normalized Born ratio and corresponds to the value on the left side of Eq. (1). W_T and W_B are the weight

matrices for the target and background regions, respectively. $[X_T]$ and $[X_B]$ are the vector representation of the distribution of total fluorophore concentrations in the target and background regions, respectively. By using this dual-zone mesh, the total number of voxels with the unknown concentration can be maintained on the same scale of the total number of measurements. As a result, the inverse problem is less underdetermined. Thus, dual-zone mesh schedule significantly improves the fluorophore quantification and target-to-background contrast. The total least-square method and the conjugate gradient technique were used to iteratively solve Eq. (2).³⁴ In the experiments, the tumor target depth or region can be estimated from US or a depth estimation algorithm reported in Ref. 24. In this study, we have used US image to provide the target depth before placing the mouse in the Intralipid solution.

3 Results

3.1 VEGFR-2-Mediated Binding of scVEGF-Lip/ICG In Vitro

Upon binding to VEGFRs, VEGF rapidly induces receptor dimerization and tyrosine autophosphorylation that is readily detectable in VEGFR-overexpressing cells.²² We evaluated the ability of scVEGF-Lip/ICG to bind to VEGF receptor (VEGFR-2), as measured by induction of VEGFR-2 tyrosine autophosphorylation in 293/KDR cells engineered to express $\sim 2.5 \times 10^5$ VEGFR-2/cell. We found that in a short-term 10-min assay, scVEGF-Lip/ICG induced VEGFR-2 tyrosine autophosphorylation at low nanomolar concentrations, which was comparable with that of free scVEGF, albeit the saturation of the tyrosine phosphorylation signal was reached at an approximately fivefold higher concentration of liposomal versus free scVEGF [Fig. 2(a)].

Binding of scVEGF-Lip/ICG to VEGFR-2 was also validated in a long-term 96-h assay, where scVEGF-Lip/ICG competed with a previously described recombinant chimeric cytotoxin, SLT-VEGF. This toxin accumulates in 293/KDR cells via VEGFR-2 mediated endocytosis and kills the cells during 24 to 48 h of exposure, unless it is competed out by scVEGF or scVEGF-based constructs.¹⁹ We found that scVEGF-Lip/ICG protected 293/KDR cells, although with IC₅₀ somewhat higher than that for parental scVEGF [Fig. 2(b)]. Thus, both assays indicated that scVEGF tethered to the liposomal surface via a PEGylated lipid retains the ability to bind to VEGFR-2. The higher saturating concentrations of liposome-associated scVEGF in both assays most likely reflect the fact that only a fraction of liposomal scVEGF that is located on the liposome–cell interface is available for interaction with cellular receptors.

We next used PAE/KDR, porcine endothelial cells, engineered to overexpress VEGFR-2²² and flow cytometry to explore binding and potential receptor-mediated internalization of scVEGF-Lip/ICG. PAE/KDR cells were incubated with scVEGF-Lip/ICG or untargeted Lip/ICG at matching concentrations of ICG or without fluorescent tracer. After 1 h of incubation at 37°C, cells were extensively washed with PBS, including a high-salt wash with PBS supplemented with 0.5-M NaCl, detached, fixed with PFA, and the presence of cell-associated ICG was analyzed by flow cytometry [Fig. 2(c)]. We found that PAE/KDR cells incubated with targeted scVEGF-Lip/ICG displayed significantly higher ICG fluorescence than those incubated with Lip/ICG or without tracer (the mean

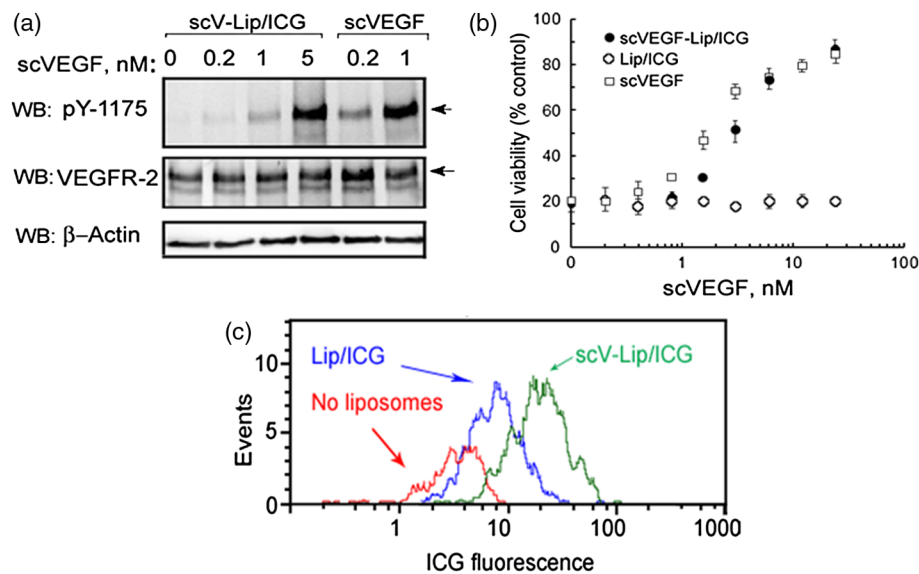


Fig. 2 Functional activity of scVEGF site-specifically attached to Lip/ICG. (a) Lysates of 293/KDR cells after a 10-min stimulation with the indicated amounts of liposomal or free scVEGF were separated by SDS-PAGE on 7.5% gels to analyze tyrosine phosphorylation of Y1175 residue in VEGFR-2 (top) and total VEGFR-2 (middle) or on 15% gels to analyze β -actin (loading control, bottom) by Western blotting (WB). Errors indicate positions of VEGFR-2. (b) Cell viability after a 96-h exposure of 293/KDR cells to 1-nM SLT-VEGF in the presence of varying amounts of scVEGF-Lip/ICG, nontargeted Lip/ICG, or free scVEGF. The numbers of viable naïve cells in control untreated wells were taken as 100%. (c) Flow cytometry analysis of liposome accumulation in PAE/KDR cells after 1 h of incubation. Green, scVEGF-Lip/ICG; blue, nontargeted Lip/ICG; and red, naïve cells.

fluorescence values of 22.3 versus 8.8 versus 3.7, respectively). Although our experiments did not distinguish between VEGFR-2 bound and internalized scVEGF-Lip/ICG, VEGFR-2-mediated internalization was reported previously for other scVEGF-driven liposomes and dendrimers.^{23,31} Taken together, three *in vitro* assays indicate that scVEGF-Lip/ICG displays a significant receptor-binding ability of scVEGF and are capable of accumulating in endothelial cells expressing high levels of VEGFRs.

3.2 FDOT Imaging of Orthotopic Tumors with scVEGF-Lip/ICG and Control Tracers

For imaging experiments *in vivo*, we used a previously described 4T1luc orthotopic mouse breast cancer model with VEGFR overexpressed on endothelial cells in angiogenic tumor vasculature formed by the mouse host.²² In this model, the predominant VEGFR expressed on tumor endothelial cells is VEGFR-2, which binds human VEGF and its scVEGF derivative, which allows for *in vivo* imaging with scVEGF-based tracers.²² 4T1luc mouse breast carcinoma cells were injected into mouse mammary fatpad of syngeneic female Balb/c mice, and after 2 to 3 weeks, highly vascularized 6- to 7-mm tumors were readily observed. Tumor-bearing mice were used for imaging experiments, in which imaging depth (separation between imaging probe and the surface of the tumor) was 1.5 cm. Mice were randomized into four groups and after the background fluorescence was measured, each group was intravenously injected with the same amount of ICG/mouse (5 nmol) using the following formulations: targeted scVEGF-Lip/ICG ($n = 6$), untargeted Lip/ICG ($n = 6$), inactive-Lip/ICG decorated with functionally inactive scVEGF ($n = 3$), and free ICG ($n = 3$).

Figure 3 shows typical longitudinal sets of fluorescent images obtained by FDOT over a 400-min period for an individual mouse injected with scVEGF-Lip/ICG [Fig. 3(a)], Lip/ICG [Fig. 3(b)], inactive-Lip/ICG [Fig. 3(c)], and free ICG [Fig. 3(d)]. Each image is 6×6 cm² in x and y spatial dimensions at the corresponding target depth, and the color bar represents the reconstructed dye concentration in micromolar. All tracers accumulated in and cleared from the tumor area with visibly different rates, reflecting tracer-specific uptake mechanisms. The patterns of tracer uptake in the tumor were further analyzed using reconstructed maximum fluorescence concentrations in micromolar from each mouse at all observation points with a subtracted background fluorescence equivalent to 0.06 μ M. The mean values of the maximum fluorescence concentrations of all mice at each observation point were calculated, and the exponential fitting of these values for washout periods is shown in Figs. 4(a) and 4(b). We found that, for targeted scVEGF-Lip/ICG tracer, this parameter reached maximum of 0.109 μ M at 30-min postinjection, and the signal remained above the detection level for at least 4 h with a half-life of \sim 90 min. By contrast, the untargeted Lip/ICG reached its maximum value of 0.091 μ M approximately twice as fast (15-min versus 30-min postinjection) and declined threefold faster with a half-life time of \sim 30 min. The results obtained for inactive-Lip/ICG were similar to those for Lip/ICG (maximum fluorescence concentration 0.08 μ M, maximum accumulation at 15-min postinjection, and the signal declining below detection level by \sim 3 h with half-life time of \sim 33 min). Interestingly, for free ICG, fluorescence concentration reached a lower maximum of 0.053 μ M at 15-min postinjection, and then the signal declined significantly faster than for any liposomal formulation below the detection level by \sim 60-min postinjection with a half-life time of \sim 23 min.

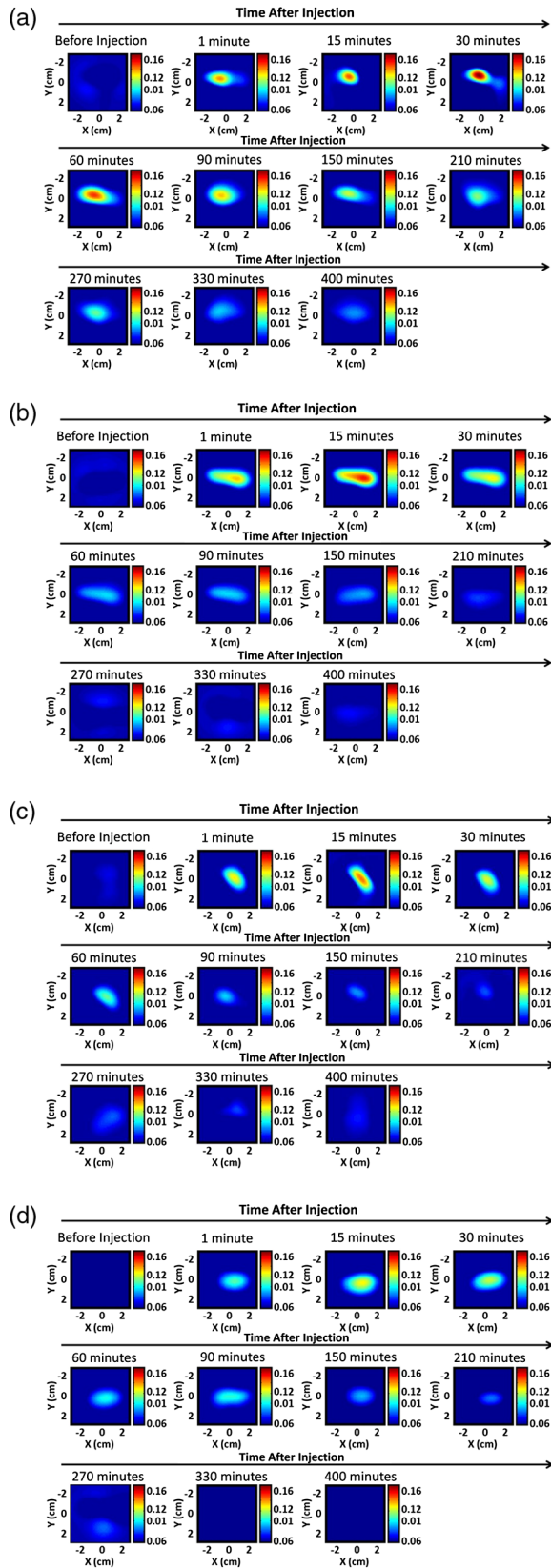


Fig. 3 Examples of longitudinal fluorescence tomography images obtained at different time points between 1 and 400 min after injection of 5 nmol ICG/mouse formulated as (a) targeted scVEGF-Lip/ICG with ~5 pmol of scVEGF, (b) untargeted Lip/ICG, (c) inactive-Lip/ICG, (d) free ICG and monitored for 400 min. The tumors were located at approximately 1.5 cm.

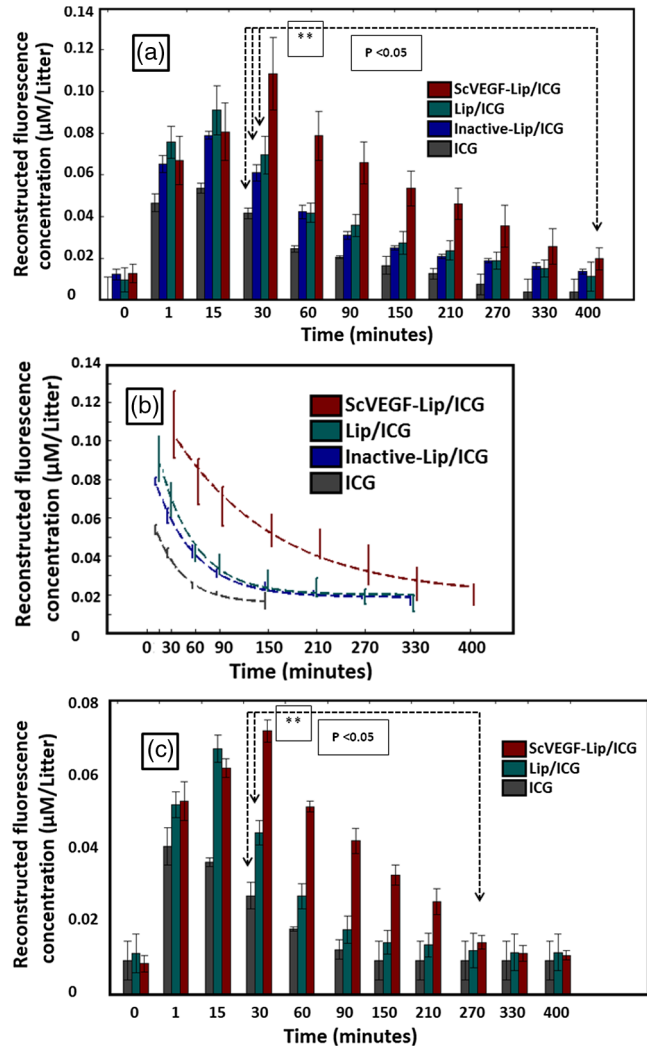


Fig. 4 Kinetics of tumor uptake of free ICG, inactive-Lip/ICG (1.5 cm only), nontargeted Lip/ICG, and targeted scVEGF-Lip/ICG. Reconstructed maximum fluorescence concentration for tumors located at (a) 1.5-cm and (c) 2-cm imaging depths. All tracers were injected at 5 nmol ICG/mouse. The exponential fitting of the washout period for each tracer is also shown for 1.5-cm imaging depth (b). ***P*-values were computed at each time point between targeted scVEGF-Lip/ICG and three control groups within this time window.

Similar patterns of tracer uptake and clearance were observed in separate experiments with imaging depths of 2 cm [Fig. 4(c)]. Although the maximum signals were approximately twofold lower than those at 1.5-cm imaging depth, the accumulation and clearance of scVEGF-Lip/ICG tracer were significantly slower than those for Lip/ICG or free ICG.

To validate that the registered FDOT signals were originated from the tumors as opposed to those from the internal organs, one mouse was intravenously injected with 5 nmol of targeted scVEGF-Lip/ICG and then imaged for 30 min, a time of maximum tracer uptake. After that mouse was sacrificed, the tumor was rapidly removed surgically, and the tumor-free mouse was reimaged. A longitudinal set of fluorescent images obtained in the course of this experiment showed that the accumulated fluorescent signal in the tumor area was decreased almost to the background level after the tumor removal, eliminating the possibility that it was associated with any of the internal organs (Fig. 5).

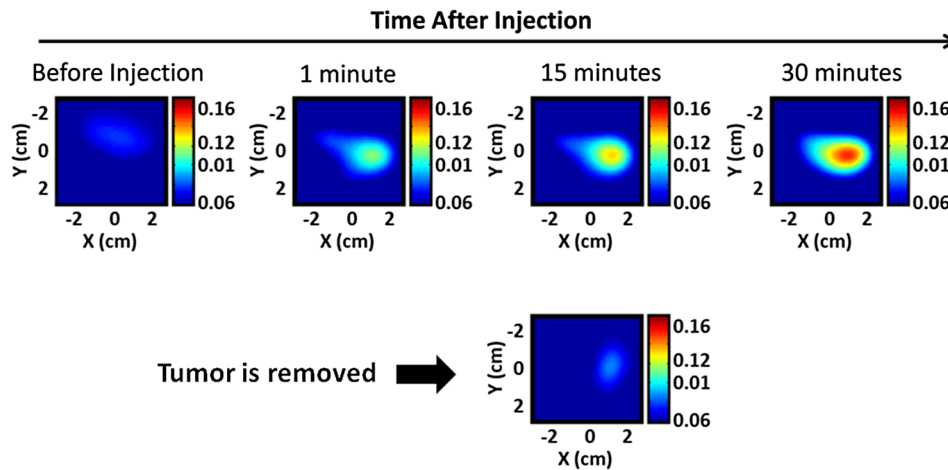


Fig. 5 Longitudinal fluorescence tomography images obtained at different time points over a 30-min period (the maximum uptake) and immediately after removal of the tumor at 30 min. Mouse was injected with 5 nmol ICG/mouse of targeted scVEGF-Lip/ICG, and tumor was located at approximately 1.5 cm.

The significantly higher persistent uptake of targeted scVEGF-Lip/ICG versus untargeted Lip/ICG, inactive-Lip/IC, or free ICG was confirmed by analyses of fluorescence on cryosections obtained from tumors harvested from tracer-injected mice at 400-min postinjection. For each tumor, several cryosections were taken at different locations including top, middle, and bottom of the tumor. Fluorescence images for these cryosections

were obtained using Odyssey Imager (LI-COR). Representative images of four cryosections separated by ~ 2 -mm cutting distance and H&E-stained images for the first section of each group are shown in Fig. 6 for each tracer. Qualitatively, at 400-min postinjection, the signal obtained with scVEGF-Lip/ICG was visibly stronger than those obtained with Lip/ICG or inactive-Lip/ICG, whereas no signal was detected on

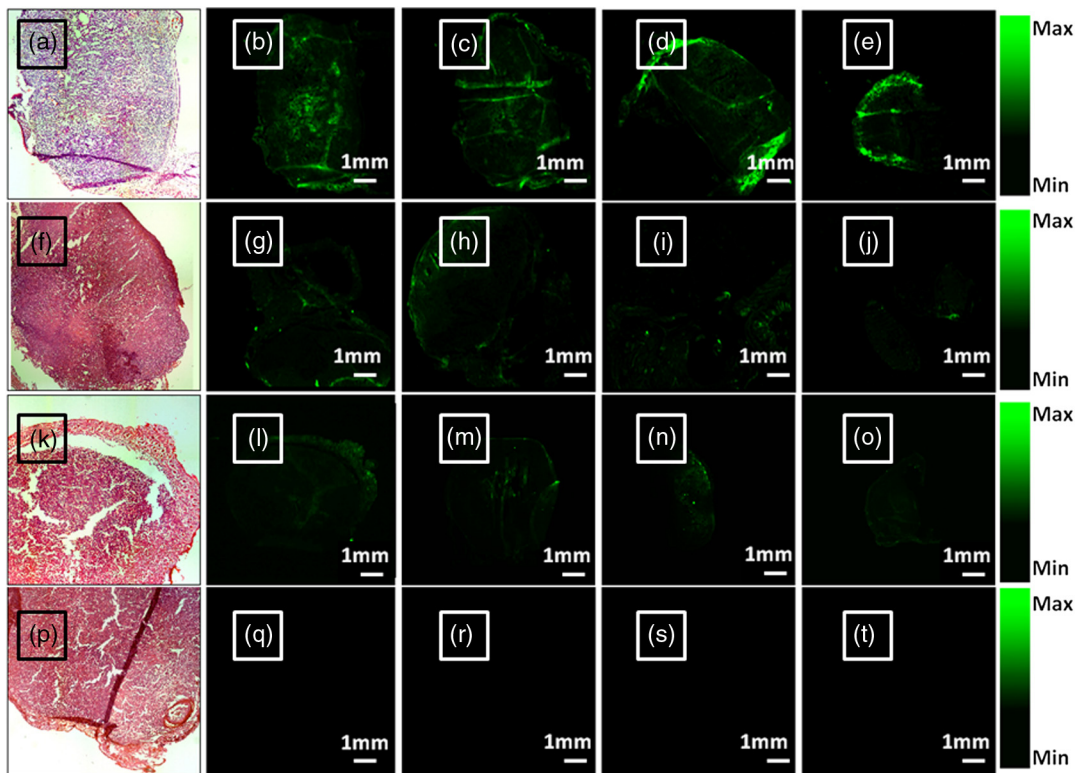


Fig. 6 H&E and *ex vivo* fluorescence images of cryosections from tumors harvested at 400-min postinjection. (b–e) Images of four cryosections of the harvested tumor from mouse injected with 5 nmol ICG/mouse of targeted scVEGF-Lip/ICG. (g–j) Images of four cryosections of the harvested tumor from mouse injected with 5 nmol ICG/mouse of nontargeted Lip/ICG. (l–o) Images of four cryosections of the harvested tumor from mouse injected with 5 nmol ICG/mouse of inactive-Lip/ICG. (q–t) Images of four cryosections of the harvested tumor from mouse injected with 5 nmol ICG/mouse of free ICG. (a, f, k, p) H&E images corresponding to the first slice of each group.

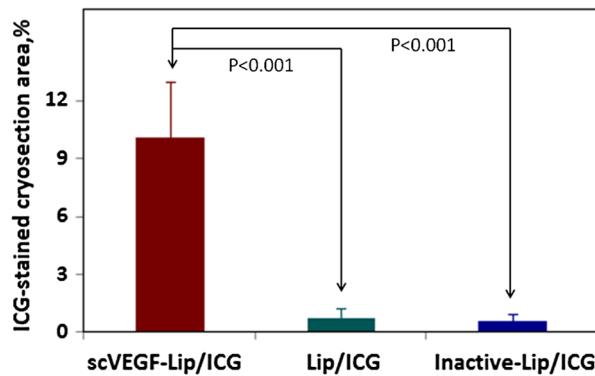


Fig. 7 Prevalence of ICG staining on cryosections from tumors harvested from three sets of mice injected with 5 nmol ICG/mouse of targeted scVEGF-Lip/ICG, nontargeted Lip/ICG, and inactive-Lip/ICG. $P = 0.0006$ for difference between targeted and other Lip/ICG formulations.

cryosections obtained from free-ICG injected mice. To further quantify these differences, the percentage of pixels with ICG signal above the same threshold level was determined for each image in the large set of images for each group. As shown in Fig. 7, the percentage of pixels with ICG signal for the targeted scVEGF-Lip/ICG-injected group was approximately 15-fold higher ($10.1\% \pm 2.8\%$) than that for both untargeted formulations Lip/ICG and inactive-Lip/ICG ($0.7\% \pm 0.5\%$ and $0.6\% \pm 0.4\%$).

4 Discussion and Summary

FDA-approved fluorescent dye ICG is widely used for various diagnostic applications including recent efforts to extend its use for breast cancer diagnostics.³⁵ Although ICG binds to blood proteins and these complexes are transiently entrapped in tumors via EPR effect associated with leaky tumor vasculature, the rate of blood clearance is very high ($t_{1/2}$ of ~25 min in humans) and the narrow observation window leads to various logistical difficulties in monitoring ICG fluorescent signal in tumors. EPR-based accumulation can be enhanced for ICG-encapsulating liposomes (Lip/ICG) relative to albumin/ICG complexes; however, Lip/ICG cannot penetrate beyond one or two subendothelial layers of cells after extravasation through tumor endothelium, and typically are efficiently cleared by tumor resident macrophages. Here, we tested the hypothesis that targeting liposome-encapsulating ICG (Lip/ICG) to VEGFR, receptors overexpressed on tumor endothelial cells and readily accessible from the bloodstream, may provide better imaging than using Lip/ICG compositions that can accumulate in tumor only via EPR effects. For targeting Lip/ICG to VEGFR, we used an engineered version of VEGF, scVEGF, which was tethered to liposome surface via a site-specifically conjugated PEGylated lipid. This targeting ligand was validated previously with a number of imaging and therapeutic constructs, providing effective binding to VEGFR and a possibility of VEGFR-mediated endocytosis.^{25,26,36}

Indeed, we found that in three different assays with cells overexpressing VEGFR-2, scVEGF-Lip/ICG, at concentrations of scVEGF in a nanomolar range, readily bound to the receptors (Fig. 2). Although saturating concentrations of liposomal scVEGF were higher than those for free scVEGF, these differences are not surprising, as only a fraction of liposomal surface with tethered scVEGF can be in contact with the cell surface. Although we did not specifically explore VEGFR-2-mediated endocytosis of scVEGF-Lip/ICG, previous

experience with scVEGF-driven therapeutic liposomes suggests that such a process could take place.³⁶

After intravenous injection of tracers, we employed longitudinal FDOT imaging of individual mice for monitoring the dynamics of fluorescent signals in the area of orthotopic mouse breast carcinoma. Virtual elimination of the fluorescent signal after surgical removal of the tumor at 30 min after tracer injection (Fig. 5) excluded the possibility that the detected signals in our experiments were originated not from the tumors but from the internal organs. In longitudinal experiments, as expected for EPR-based tracer accumulation, we found that Lip/ICG-associated fluorescent signal was higher and declined slower than that from of ICG, presumably bound to blood albumins. However, relative to untargeted Lip/ICG, the VEGFR-targeted scVEGF-Lip/ICG tracer provided for slower (30 min versus 15 min) increase and a remarkably more sustainable tumor-associated fluorescent signal with a half-life of 90 min versus 30 min (Figs. 3 and 4). Hypothetically, scVEGF-Lip/ICG could also accumulate in tumor via EPR effect, and the differences in sustainable fluorescent signal could be due to the changes in EPR effects caused by the shell formed by PEGylated scVEGF tethered to Lip/ICG. However, such an explanation appears unlikely because the signal dynamic obtained with inactive-Lip/ICG (decorated with inactivated scVEGF) is very similar to that of untargeted Lip/ICG. Enhanced retention of scVEGF-Lip/ICG initiated signals was further confirmed by the direct analysis of fluorescence on the cryosections from tumors harvested at 6 h after injection. Importantly, this significant long-term difference in retention of targeted versus untargeted tracers suggests that receptor-mediated endocytosis of scVEGF-Lip/ICG might take place. However, a different study combining kinetic analysis and extensive fluorescent microscopy would be required to validate or disprove this suggestion.

Taken together, our findings support the hypothesis that scVEGF-Lip/ICG tracer targeted to VEGFR may significantly expand the window for fluorescent tumor imaging relative to tracers that rely on EPR effects for tumor accumulation. Moreover, since overexpression of VEGFR is a rather common feature of tumor vasculature, imaging these receptors opens broader diagnostic imaging opportunities than targeting receptors that are more specific for subsets of tumor or endothelial cells. Importantly, FDOT methodology with scVEGF-Lip/ICG might be applicable to imaging lesions in biological tissues located in the depth range of 2 cm. Another potential application of scVEGF-Lip/ICG might be imaging in the tumor surgery field, where rapid assessment of the boundaries of angiogenic tumor vasculature might be useful for tumor margin demarcation. Furthermore, VEGFRs are the targets of the majority of approved and experimental antiangiogenic drugs, which affect VEGFR prevalence through not yet fully understood mechanisms; therefore, VEGFR imaging with scVEGF-Lip/ICG might be useful not only for diagnostics, but also for image-guided therapy.²⁵ These potential translation pathways for scVEGF-Lip/ICG are also supported by the recent toxicology study in mice of another scVEGF derivative, scVEGF-PEG-DOTA, conducted at a preclinical toxicology CRO in compliance with U.S. FDA Good Laboratory Practice (GLP) Regulations for Non-clinical Laboratory Studies (21 CFR Part 58). This study found no negative systemic effect at scVEGF doses of 0.5 and 4.5 mg/kg. Considering that imaging with scVEGF-Lip/ICG was performed at scVEGF doses less than 0.1 mg/kg, we are

cautiously optimistic regarding the safety aspect of translational efforts.

Acknowledgments

The authors thank graduate student Hai Li in Optical and Ultrasound Imaging Lab for some data processing. The funding was partially supported by National Institute of Health (R01EB002136 and 1R43EB012914—01A1).

References

- R. E. Nothdurft et al., "In vivo fluorescence lifetime tomography," *J. Biomed. Opt.* **14**(2), 024004 (2009).
- Y. Lin et al., "In vivo validation of quantitative frequency domain fluorescence tomography," *J. Biomed. Opt.* **17**(12), 126021 (2012).
- K. M. Tichauer et al., "Computed tomography-guided time-domain diffuse fluorescence tomography in small animals for localization of cancer biomarkers," *J. Visualized Exp.* **17**(65), e4050 (2012).
- C. D. Darné et al., "A compact frequency-domain photon migration system for integration into commercial hybrid small animal imaging scanners for fluorescence tomography," *Phys. Med. Biol.* **57**(24), 8135–8152 (2012).
- P. Y. Fortin et al., "Detection of brain tumors using fluorescence diffuse optical tomography and nanoparticles as contrast agents," *J. Biomed. Opt.* **17**(12), 126004 (2012).
- M. Solomon et al., "Video-rate fluorescence diffuse optical tomography for in vivo sentinel lymph node imaging," *Biomed. Opt. Express* **2**(12), 3267–3277 (2011).
- F. Leblond et al., "Toward whole-body optical imaging of rats using single-photon counting fluorescence tomography," *Opt. Lett.* **36**(19), 3723–3725 (2011).
- A. Corlu et al., "Three-dimensional in vivo fluorescence diffuse optical tomography of breast cancer in humans," *Opt. Express* **15**(11), 6696–6716 (2007).
- S. J. Erickson et al., "Three-dimensional fluorescence tomography of human breast tissues in vivo using a hand-held optical imager," *Phys. Med. Biol.* **58**(5), 1563–1679 (2013).
- A. Poellinger et al., "Near-infrared imaging of the breast using omocyanine as a fluorescent dye: results of a placebo-controlled, clinical, multicenter trial," *Invest. Radiol.* **46**(11), 697–704 (2011).
- E. M. Sevic-Muraca et al., "Advancing the translation of optical imaging agents for clinical imaging," *Biomed. Opt. Express* **4**(1), 160–170 (2013).
- A. Taruttis and V. Ntziachristos, "Translational optical imaging," *AJR Am. J. Roentgenol.* **199**(2), 263–271 (2012).
- A. Y. Sajjadi, K. Mitra, and M. S. Grace, "Short-pulse laser-based system for detection of tumors: administration of gold nanoparticles enhances contrast," *J. Nanotechnol. Eng. Med.* **3**(2), 021002 (2012).
- R. C. Benson and H. A. Kues, "Fluorescence properties of indocyanine green as related to angiography," *Phys. Med. Biol.* **23**(1), 159–163 (1978).
- S. Zanganeh et al., "Photoacoustic imaging enhanced by indocyanine green-conjugated single-wall carbon nanotubes," *J. Biomed. Opt.* **18**(9), 096006 (2013).
- H. Maeda et al., "Tumor vascular permeability and the EPR effect in macromolecular therapeutics: a review," *J. Control. Release* **65**(1–2), 271–284 (2000).
- B. Ebert et al., "Cyanine dyes as contrast agents for near-infrared imaging in vivo: acute tolerance, pharmacokinetics, and fluorescence imaging," *J. Biomed. Opt.* **16**(6), 066003 (2011).
- F. P. Navarro et al., "Lipid nanoparticle vectorization of indocyanine green improves fluorescence imaging for tumor diagnosis and lymph node resection," *J. Biomed. Nanotechnol.* **8**(5), 730–741 (2012).
- S. T. Proulx et al., "Quantitative imaging of lymphatic function with liposomal indocyanine green," *Cancer Res.* **70**(18), 7053–7062 (2010).
- E. Portnoy et al., "Cetuximab-labeled liposomes containing near-infrared probe for in vivo imaging," *Nanomedicine* **7**(4), 480–488 (2011).
- W. C. Zamboni et al., "Tumor disposition of pegylated liposomal CKD-602 and the reticuloendothelial system in preclinical tumor models," *J. Liposome Res.* **21**(1), 70–80 (2011).
- M. V. Backer et al., "Molecular imaging of VEGF receptors in angiogenic vasculature with single-chain VEGF-based probes," *Nat. Med.* **13**(4), 504–509 (2007).
- B. T. Thirumagal et al., "Receptor-targeted liposomal delivery of boron-containing cholesterol mimics for boron neutron capture therapy (BNCT)," *Bioconjug. Chem.* **17**(5), 1141–1150 (2006).
- N. C. Biswal et al., "Fluorescence imaging of vascular endothelial growth factor in tumors for mice embedded in a turbid medium," *J. Biomed. Opt.* **15**(1), 016012 (2010).
- M. V. Backer and J. M. Backer, "Imaging key biomarkers of tumor angiogenesis," *Theranostics* **2**(5), 502–515 (2012).
- M. V. Backer et al., "Cysteine-containing fusion tag for site-specific conjugation of therapeutic and imaging agents to targeting proteins," *Methods Mol. Biol.* **494**(1), 275–294 (2008).
- C. R. Anderson et al., "scVEGF Microbubble ultrasound contrast agents: a novel probe for ultrasound molecular imaging of tumor angiogenesis," *Invest. Radiol.* **45**(10), 579–585 (2010).
- M. M. Tedesco et al., "Analysis of in situ and ex vivo vascular endothelial growth factor receptor expression during experimental aortic aneurysm progression," *Arterioscler. Thromb. Vasc. Biol.* **29**(10), 1452–1457 (2009).
- J. Zhang et al., "Molecular imaging of vascular endothelial growth factor receptors in graft arteriosclerosis," *Atheroscler. Thromb. Vasc. Biol.* **32**(8), 1849–1855 (2012).
- Z. Levashova et al., "Imaging VEGF receptors in turpentine induced sterile thigh abscesses using radiolabeled scVEGF," *J. Nucl. Med.* **50**(12), 2058–2063 (2009).
- Y. Xu et al., "Targeting tumor hypoxia with 2-nitroimidazole-ICG dye conjugates," *J. Biomed. Opt.* **18**(6), 066009 (2013).
- V. Ntziachristos and R. Weissleder, "Experimental three-dimensional fluorescence reconstruction of diffuse media by use of a normalized Born approximation," *Opt. Lett.* **26**(12), 893–895 (2001).
- A. Soubret, J. Ripoll, and V. Ntziachristos, "Accuracy of fluorescent tomography in the presence of heterogeneities: study of the normalized Born ratio," *IEEE Trans. Med. Imaging* **24**(10), 1377–1386 (2005).
- Q. Zhu, N. G. Chen, and S. Kurtzman, "Imaging tumor angiogenesis using combined near infrared diffusive light and ultrasound," *Opt. Lett.* **28**(5), 337–339 (2003).
- A. Poellinger et al., "Breast cancer: early- and late-fluorescence near-infrared imaging with indocyanine green—a preliminary study," *Radiology* **258**(2), 409–416 (2011).
- M. V. Backer et al., "Vascular endothelial growth factor selectively targets boronated dendrimers to tumor vasculature," *Mol. Cancer Ther.* **4**(9), 1423–1429 (2005).